

# Toughness measurement of thin films: a critical review

Sam Zhang\*, Deen Sun, Yongqing Fu, Hejun Du

*School of Mechanical and Production Engineering, Nanyang Technological University 50 Nanyang Avenue, Singapore 639798, Singapore*

Available online 8 December 2004

## Abstract

At present, there is neither standard test procedure nor standard methodology for assessment of toughness of thin films. However, researchers have long been trying to make such measurements, thus a spectrum of test methods have been developed, mostly each in its own way. As qualitative or semiquantitative assessment, a simple plasticity measurement or scratch adhesion test can mostly suffice. For quantitative description, however, a choice of bending, buckling, indentation, scratching, or tensile test has to be made. These testing methods are either stress-based or energy-based. This paper gives a critical review on these methods and concludes that, for thin films, the energy-based approach, especially the one independent of substrate, is more advantageous.

© 2004 Elsevier B.V. All rights reserved.

PACS: 68.55.-a; 68.90.+g; 68.35.Gy

Keywords: Toughness; Toughness measurement; Thin films; Coatings

## 1. Introduction

In essence, toughness is the ability of a material to absorb energy during deformation up to fracture [1,2]. Fracture toughness is the ability of a material to resist the growth of a preexisting crack. According to this definition, toughness encompasses the energy required both to create the crack and to enable the crack to propagate until fracture, whereas fracture toughness takes only account of the energy required to facilitate the crack propagation to fracture. These are two different concepts and should not be confused and interchangeably used. For bulk materials and some thick films, fracture toughness is easily measured according to ASTM standards [3,4]. However, for thin films, fracture toughness measurement remains difficult because of the thickness limitation [5]. As thin films are increasingly finding their way in engineering applications, thin film toughness assessment becomes imperative. Unlike the bulk materials, however, until now, there is neither standard procedure nor commonly accepted methodology to follow. It is, however, good to note that increasing efforts have been made to address this tricky issue, and thus quite many test

methods are proposed and used in various literatures. This paper attempts to size up these methods, compare, and sort out the critical issues. An effort is made to confine the scope to hard and superhard thin films (thus, soft thin films fall out of the scope). To avoid unnecessary complication, the word “films” is used in this paper to mean films as well as coatings.

## 2. Toughness measurement methodologies

The methodologies employed to measure toughness for thin films fall into one of these methods: bending, buckling, scratching, indentation, and tensile tests, which are discussed in details below.

### 2.1. Bending

For freestanding thick films of tens or hundreds of microns in thickness, measurement of the fracture toughness can be very similar to that for a bulk material: creating a precrack, applying a stress to induce crack propagation, and then measuring the critical stress needed to inflict fracture. However, introduction of a precrack of known size in a film, especially in a thin film of only

\* Corresponding author. Tel.: +65 6790 4400; fax: +65 6791 1859.

E-mail address: [msyzhang@ntu.edu.sg](mailto:msyzhang@ntu.edu.sg) (S. Zhang).

micron size or submicron size thick, is extremely tricky. In Ref. [6], a freestanding diamond film with thickness in the order of millimeters was laser-cut at one edge to form a notch and then glued onto the side face of a brass beam (cf. Fig. 1). The brass beam was bent so that a precrack was generated in the film at the end of the notch. The film was then removed from the beam and put under a three-point flexure to bend, as illustrated in Fig. 2.

The fracture toughness was thus calculated according to ASTM standard E-399 [3] using

$$K_{Ic} = \left( P_c S / h W^{2/3} \right) f(a/W) \quad (1)$$

where  $P_c$  is the load at fracture,  $h$  and  $W$  are the thickness and the width of the film, respectively,  $S$  is the span between the two supporting positions, and  $a$  is the length of the preexisting crack,  $f$  is a function of  $a/W$ . That is not an easy experiment, let alone the possible errors easily introduced during gluing and ungluing, nonsymmetrical propagation of crack in the brass plates, etc. Obviously, this method is not applicable for thin films.

Jaeger et al. [7] used an ingenious way to make the precrack: a notch was first made on the front face of the steel substrate, and a hole was bored at the end (cf. Fig. 3). The substrate was then fatigued to generate a crack from the notch that propagated and stopped at the hole. After that, a few-micron-thick film was deposited onto the side faces of the substrate. The coated substrate then underwent two successive four-point bending tests: one in the as-coated state, the other after the film was broken. During the bending, the load was recorded as a function of the displacement. When the crack reached the hole, the load was removed and then replaced for the second flexure. The second bending was stopped as the displacement reached the value of the first bending. The difference in load  $F$  was considered the load required for crack propagation in the film. During the two successive bending processes, if the substrate remained elastic, the energy difference ( $\Delta U_e$ ) would represent the energy required to enable cracking of

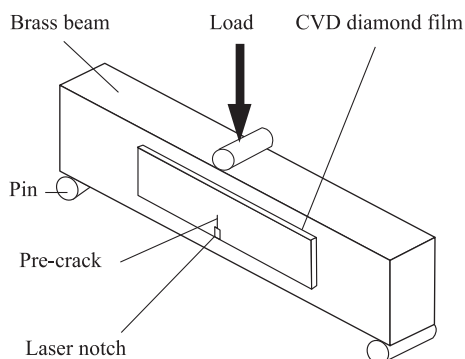


Fig. 1. Schematic diagram of introducing precrack in film using bending method [6].

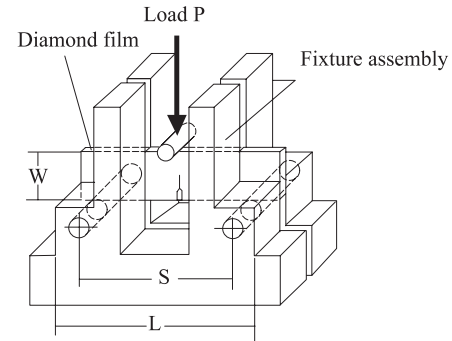


Fig. 2. Schematic diagram of three-point bending test of a freestanding diamond films with precrack [6].

the film. The critical energy release rate  $G_c$  can be written as

$$G_c = - \frac{dU_e}{dA} = - \frac{\frac{1}{2} F^2 \cdot dC}{2h \cdot da} \quad (2)$$

where  $U_e$  is the elastic energy,  $A$  is the area of the crack,  $h$  is the film thickness,  $dC/da$  is the change in the compliance ( $C$ ) of the film with respect to the change in crack length ( $a$ ),  $F$  is the measured force difference from the two successive bending. Under the plain stress condition (that is, the film thickness is significantly less than length and width), fracture toughness  $K_{Ic}$  can be calculated from  $G_c$  through

$$K_{Ic} = \sqrt{EG_c} \quad (3)$$

Testing of TiN, TiCN, and TiAlN films of 4.8 to 7.9  $\mu\text{m}$  thick [deposited via plasma-assisted chemical vapor deposition (PACVD)] yields a fracture toughness of these films as 8.7, 7.9, and 3.8  $\text{MPa m}^{1/2}$ , respectively. However, as the authors readily pointed out, the introduction of precrack into substrate may have significant effects on film formation and growth during deposition process, therefore affecting the fracture toughness values. In addition, should there be any plastic deformation in the substrate, energy

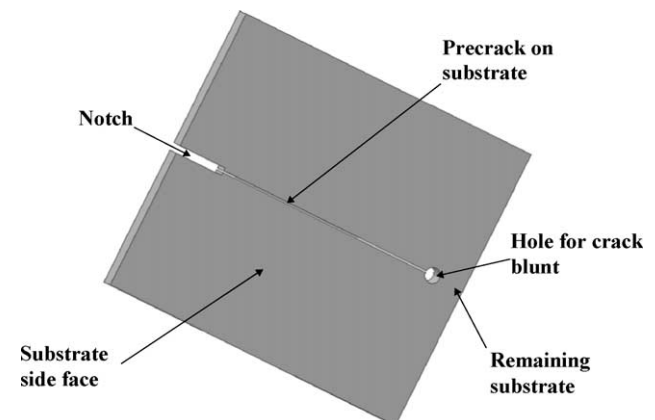


Fig. 3. Substrate with precrack for hard thin film toughness measurement via four-point bending; the film will be deposited on the side face.

measurement would be wrong, and thus affecting the toughness calculation.

Preparation of precise precrack in films is usually difficult and inconvenient. This is especially true for hard films with thickness of microns or submicrons. Therefore, bending without precrack is adopted by some researchers [8–10], and “cracking resistance” is indirectly used as a measure of fracture toughness. The cracking resistance is defined as the threshold strain over which density of the crack sharply increases. The onset of the increase of the number of cracks is detectable by significant increase in acoustic emission from a detector mounted on the film [11–13] or by directly measuring the crack density as a function of strain [14,15]. Installing the flexure in a scanning electron microscope (SEM) facilitates “live” monitoring of the formation of cracks [16]. Wiklund et al. [17] measured the cracking resistance of CrN (2.5  $\mu\text{m}$  thick) and TiN (4.3  $\mu\text{m}$  thick) films as 0.7% and 0.1%, respectively.

## 2.2. Buckling

Cotterell et al. [18,19] used the buckling test (cf. Fig. 4) to determine fracture toughness of indium–tin–oxide (ITO) thin films. Polyethylene Terephthalate (PET) polymer of a few tenth of millimeter in thickness was used as the substrate due to its excellent elasticity. ITO films with thickness between 80 and 140 nm were deposited on the PET substrate. The testing scheme (cf. Fig. 4) can be analyzed as a plane strain beam loaded along its axis. According to large deformation buckling theory of beams, the following equation can be obtained [20]:

$$\chi = 2 \left[ 1 - \frac{E(k)}{K(k)} \right] \quad (4)$$

$$\frac{l}{R} = 4K(k)k \quad (5)$$

where  $K(k)$  and  $E(k)$  are complete elliptic integrals,  $k = \sin(\theta/2)$ ,  $L$  is the original length of the beam,  $R$  is radius of curvature, and  $\chi = e/L$ , contraction ratio. For the two schemes in Fig. 4,  $l = L$  for simple support and  $l = L/2$  for built-in ends. The radius of bending can be calculated by measuring the shortening of the beam  $e$ . Since the ITO film is so thin compared with the substrate, the neutral axis of the composite is very near to the center of

composite. Therefore, the strain in the thin film can be given by

$$\varepsilon = \frac{h_s + h_f}{2R} \quad (6)$$

where  $h_s$  and  $h_f$  are the thickness of the substrate and film, respectively. Owing to the difference in conductivity of the substrate and the film, cracking of the film can be determined from a change in electrical conductivity. The strain just before the sudden change in resistance is taken as the critical strain  $\varepsilon_c$ , which is used to calculate the critical strain energy release rate through [21]

$$G_C = \frac{1}{2} E_f \varepsilon_c^2 \pi h_f g(\alpha, \beta) \quad (7)$$

where  $E_f$  is the elastic modulus of thin film, the factor  $g(\alpha, \beta)$  is a function of the Dundur's parameter, and the value of  $g$  factor can be computed by finite element method [22]. Since the PET polymer is used as the substrate, large elastic deformation in substrate before film fracture becomes possible. However, the low melting temperature of the polymer substrate limits the application.

## 2.3. Scratching

Scratch test is generally accepted as one of the simple means in assessing adhesion strength of a film on its substrate [23–25]. In the test process, a diamond tip is driven over a coated surface to produce a scratch. The load on the diamond tip is increased linearly to induce a shear force in the nearby film that is proportional to the applied load and transmitted through the bulk of the composite sample. As the mechanical properties of the film and the substrate are different, there is a discontinuity in the shear stress at the interface which, when sufficiently high, induces adhesive failure at a critical load. Generally, for hard thin films, microcracks appear in films during scratching before the final adhesion failure [26]. The minimum load at which the first crack occurs is termed the lower critical load  $L_{c1}$ , and the load corresponding to the complete peeling of the film is termed the higher critical load  $L_{c2}$  (cf. Fig. 5). Some researchers directly used the lower critical load to indicate cracking resistance [27,28], or some even termed it “scratch toughness” [29,30]. A magnetron sputtered  $\text{Ti}_{1-x}\text{Al}_x\text{N}$  nanocomposite thin film (hardness 28.5 GPa, thickness 0.9  $\mu\text{m}$ ) which reaches 70 N load without brittle failure at

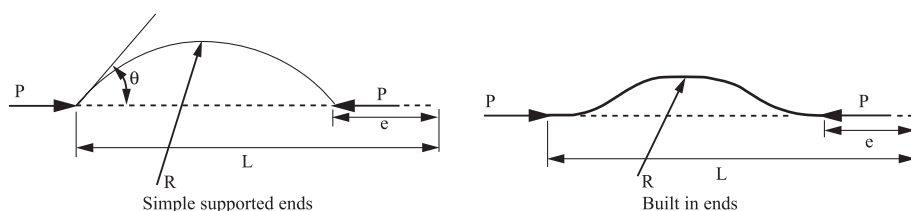


Fig. 4. Schematic illustration of buckling test. Left: simple support ends; Right: built-in ends [19].

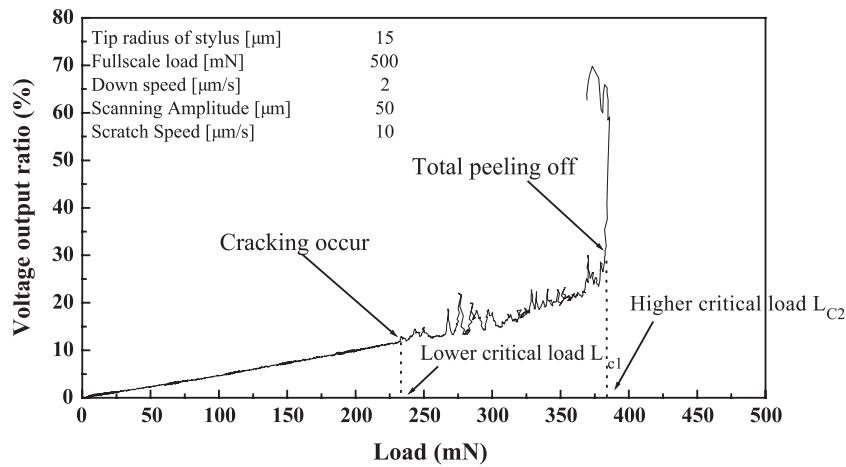


Fig. 5. Scratch adhesion profile.

Rockwell diamond tip (200  $\mu\text{m}$  in radius) is thus considered having good scratch toughness. In comparison, films of TiN (0.9  $\mu\text{m}$ ,  $L_{c1}=30\text{--}40\text{ N}$ ) and AlN (0.6  $\mu\text{m}$ ,  $L_{c1}=20\text{ N}$ ) [31] are not so good in scratch toughness. Since residual stress affects critical load, multipass scratch test is proposed where the scratch is performed in the same scratch track several times with increasing load. Let the critical load  $L_c^i$  be the critical load after the  $i$ th pass; as the difference between  $L_c^i$  and  $L_c^{i+n}$  ( $n \geq 1$ ) becomes 0, the value of  $L_c^i$  is then taken as qualitative characterization of the “scratch toughness” [32].

However, the critical load is not “fracture toughness” (and, of course, the unit is wrong for fracture toughness!). What the lower critical load represents is a load bearing capacity or crack initiation load. Maybe it can be treated as some sort of “crack initiation resistance”: the higher the  $L_{c1}$ , the more difficult it is to initiate a crack in the film. However, initiation of a crack does not necessarily result in fracture in the film; what is also important is how long the film can hold and withstand further loading before a catastrophic fracture occurs. Zhang et al. [33] pointed out that the film toughness should be proportional to both the lower critical load and the difference between the higher and the lower critical load. The product of these two terms is termed “Scratch Crack Propagation Resistance,” or  $\text{CPR}_s$ :

$$\text{CPR}_s = L_{c1}(L_{c2} - L_{c1}) \quad (8)$$

The parameter  $\text{CPR}_s$  can be used as quick qualitative indication of the film toughness or used in a quality control process for tough film. But  $\text{CPR}$  is not toughness.

Hoehn et al. [34] formulated an equation to relate scratch test data to proper fracture toughness. The model assumes that cracking in the microscratch test is a result of cracks being opened on surface by the applied pressure at the bottom of the scratch groove. The coefficient of grooving friction can be calculated as the ratio of the tangential force ( $F$ ) to normal force ( $P$ ) (cf. Fig. 6). The stress intensity solution for a mode I crack opening is thus given as

$$K_{IC} = \frac{2Pf_g}{R^2 \cot \theta} \left( \frac{a}{\pi} \right)^{1/2} \sin^{-1} \frac{R}{a} \quad (9)$$

where  $P$  is the pressure opening the crack,  $R$  is the radius of the indenter cone into the groove,  $2a$  is the total crack length, and  $f_g$  is the coefficient of grooving friction, which depends on the cone angle  $2\theta$  and can be obtained from the track width and the depth of penetration. However, this model is oversimplified, and the actual state of forces in the groove ahead and right below the tip are much more complicated and have to be taken into account for better description of the process.

More recently, Holmberg et al. [35] investigated the fracture toughness of thin films through measuring of the tensile stress, which induces the cohesion failure (i.e., generation of cracks in the film) through

$$K = \sigma \sqrt{b} f(a, b) \quad (10)$$

where  $\sigma$  is the tensile stress which induces the cracks in film during scratch obtained through a three-dimensional finite element modeling,  $a$  is the crack length, and  $b$  is the crack spacing,  $f(a, b)$  is a nondimensional function dependent on crack length  $a$  and crack spacing  $b$  measured from the scratch track (cf. Fig. 7). As  $a \gg b$ , Eq. (10) reduces to  $K_{IC} = \sigma \sqrt{b/2}$ . Since the calculation of the tensile stress  $\sigma$  involves 3-D finite element modeling and a general  $f(a, b)$  expression is not available, practical application of this method is difficult.

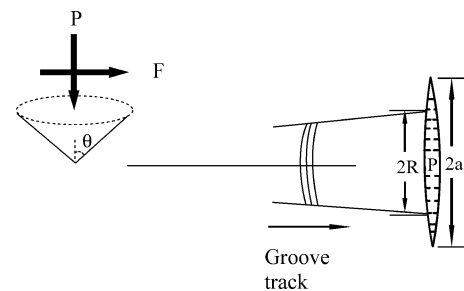


Fig. 6. Schematic diagram of the microscratch fracture toughness measurement with a pressure  $P$  opening a crack ( $2a$ ) out of a groove width  $2R$  [34].

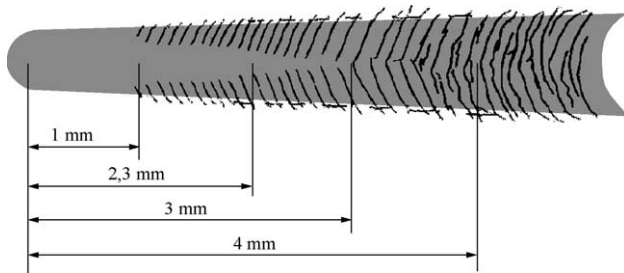


Fig. 7. Illustration of the scratch track and the cracks [35].

## 2.4. Indentation

Perhaps indentation is the most widely used tool in assessment of thin film toughness. Plastic deformation leads to stress relaxation in materials. The easier the stress relaxation proceeds, the larger plasticity is inherent in the material. Thus, comparing the plastic strain with the total strain in an indentation test directly gives a simple, rough but quick indication of how “tough” the material is. Plasticity is defined as the ratio of the plastic displacement over the total displacement in the load–displacement curve [36] (cf. Fig. 8).

$$\text{Plasticity} = \frac{\varepsilon_p}{\varepsilon} = \frac{OA}{OB} \quad (11)$$

where  $\varepsilon_p$  is the plastic deformation, and  $\varepsilon$  is the total deformation. A superhard DLC film with hardness of 60 GPa has only 10% plasticity [37], whereas a “tough” nc-TiC/a-C film with a hardness of 32 GPa has 40% plasticity [30,38]. Hydrogen-free amorphous carbon films with hardness of 30 GPa has a toughness of 50% to 60% in plasticity [39], depending on bias voltage during sputtering. Magnetron sputtered 1- $\mu\text{m}$ -thick  $\text{Ti}_{1-x}\text{Al}_x\text{N}$  films with hardness 31 GPa obtained a plasticity of 32% [31].

However, “plasticity” is not fracture toughness. To measure a film’s proper fracture toughness, Tsui et al. [40,41] introduced a precrack into the film using focused ion beam milling. The crack opening force is generated by

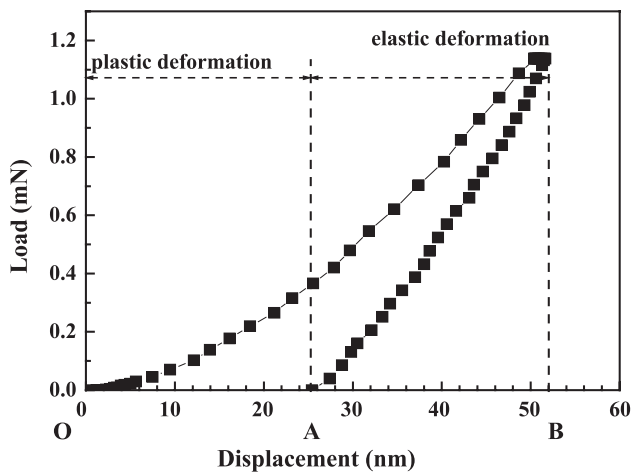


Fig. 8. Schematic plot of a load–displacement curve obtained from nanoindentation. Plasticity is calculated as OA/OB.

means of indentation sink-in effect. The sink-in effect provides a tensile stress on the film near the precrack tip and promotes the crack propagation. A Knoop indenter is used to induce a plane strain condition near the indenter. The location of the indenter and precrack is schematically shown in Fig. 9. The extent of the sink-in effect and tensile stress generated at the precrack are the largest at the center of the indentation and decrease along the elongated edges of the indentation. Thus, the crack tip opening distance and crack growth are different at different locations along the precracked trench. Under the plain strain condition, fracture toughness can be expressed as a function of crack tip blunting immediately before the catastrophic failure through the following equation

$$K_{Ic} = \sqrt{m\delta\sigma_y E} \quad (12)$$

where  $m$  is a dimensionless constant, approximately 2.0 for a plane strain condition [40,42],  $\sigma_y$  is the yield stress ( $\sigma_y \approx H/3$  [2]),  $E$  is the Young’s modulus of the films,  $\delta$  is the crack tip opening distance which is the amount of crack tip blunting before the catastrophic crack growth. The fracture toughness of NiP films with thickness of 9  $\mu\text{m}$  deposited on aluminum substrate is thus determined as 15  $\text{MPa m}^{1/2}$  [41]. The uncertainties associated with this method come from the difficulty of making the precrack and measurement of the crack tip opening distance. In addition, for films on hard substrate, the sink-in effect may not be induced that would render the method ineffective.

To avoid the difficulties in making the precrack, many researchers directly indent the films without a precrack. When the stress exceeds a critical value, a crack or spallation will be generated. Failure of the film is manifested by the formation of a kink or plateau in the load–displace-

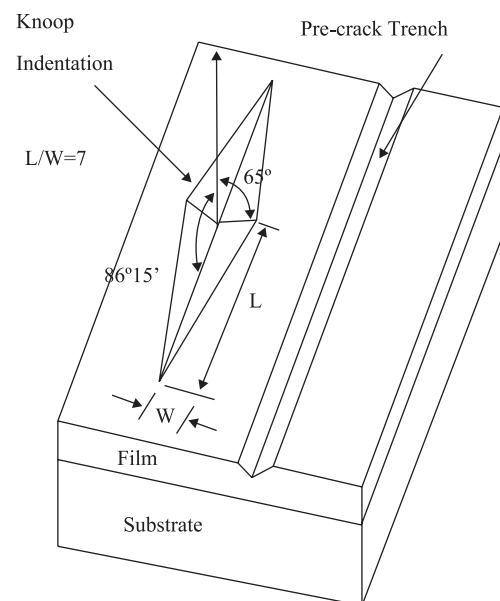


Fig. 9. Schematic illustration of the orientation of the Knoop indentation relative to the precrack trench [40].



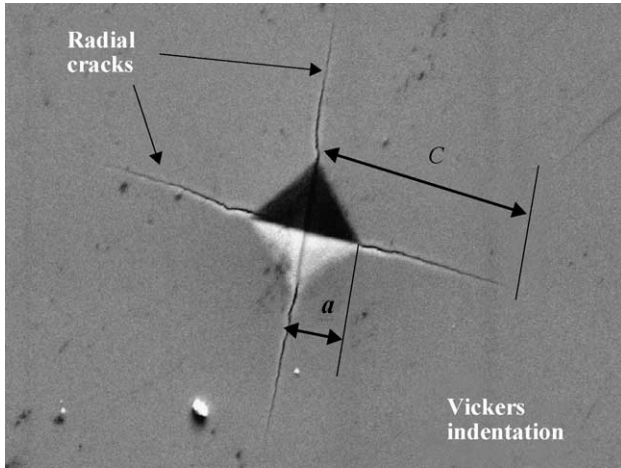


Fig. 10. SEM observation of radial cracking at Vickers indentation.

ment curve or crack formation in the indent impression [43–45]. As a qualitative, crude, and relative assessment, Holleck and Schulz [46] compare the crack length under the same load, and Kustas et al. [47] measures the “spall diameter”—the damage zone around the indenter. More quantitatively, length  $c$  of radial cracks (cf. Fig. 10) is related to the fracture toughness ( $K_{IC}$ ) through [48]:

$$K_{IC} = \delta \left( \frac{E}{H} \right)^{1/2} \left( \frac{P}{c^{3/2}} \right) \quad (13)$$

where  $P$  is the applied indentation load,  $E$  and  $H$  are the elastic modulus and hardness of the film, respectively.  $\delta$  is an empirical constant which depends on the geometry of the indenter. For standard Vickers diamond pyramid indenter and cube corner indenter, value of  $\delta$  is taken as 0.016 [49] and 0.0319 [50,51], respectively. The criterion for a well-defined crack is taken as  $c \geq 2a$  [49], where  $a$  is the half of the diagonal length of the indent. Both  $E$  and  $H$  can be determined from an indentation test at a much smaller load and analyzing of indentation load–displacement data [52]; crack length  $c$  can be obtained using SEM, thus implementation of the method seems straightforward [53].

However, the difficulty lies in the existence of a crack formation threshold, locating the indent and the determination of the crack length. Although indentation can be realized with Vickers indenter, Berkovich indenter, or cube corner indenter [54,55], there exists a cracking threshold below which indentation cracking does not occur. Existence of the cracking threshold causes severe restrictions on achievable spatial resolution. The occurrence of the indentation cracking also depends on the condition of the indenter tip [56]. Harding et al. [57] found that indentation-cracking threshold could be significantly reduced by employing a sharper indenter (cube corner indenter compared to the Berkovich and Vickers indenters). The cube corner indenter induces more than three times the indentation volume as compared to that by the Berkovich indenter at the same load. Consequently, the crack formation is easier with the

cube corner indenter, thereby reducing the cracking thresholds. For the cube corner indenter, the angle between the axis of symmetry and a face is  $35.3^\circ$  (as compared to  $65.3^\circ$  for the Berkovich indenter), and there are three cracks lying in directions parallel to the indentation diagonal (cf. Fig. 11). Cracks that are well defined and symmetrical around the cube corner indentation are used to calculate the toughness. Different researchers used different  $\delta$  values: 0.0319 [50,51], 0.040 [57], and 0.0535 [58]. Despite the inherited problems, due to its simplicity, the indentation method is widely used in toughness evaluation of thin films. To cite a few: sputter-deposited DLC film (1.92  $\mu\text{m}$  thick, 1.57  $\text{MPa m}^{1/2}$ ) [59], plasma-sprayed  $\text{Al}_2\text{O}_3$  (200–300  $\mu\text{m}$  thick, containing 13%  $\text{TiO}_2$ , 4.5  $\text{MPa m}^{1/2}$ ) [60], atmospheric pressure CVD SiC (3  $\mu\text{m}$ , 0.78  $\text{MPa m}^{1/2}$ ) [61], plasma-enhanced CVD nc-TiN/Si<sub>3</sub>N<sub>4</sub> (~1.5  $\mu\text{m}$ , 1.3–2.4  $\text{MPa m}^{1/2}$ ) [62], and  $\text{TiC}_x\text{N}_y/\text{SiCN}$  (2.7–3.3  $\mu\text{m}$ , ~1  $\text{MPa m}^{1/2}$ ) [63].

Some researchers suggest that the indentation load  $P$ , radial crack length  $c$ , and fracture toughness  $K_{IC}$  have the following relationship [64–66]:

$$\frac{P\chi_r}{c^{3/2}} = K_{IC} - 2\sigma(c/\pi)^{1/2} \quad (14)$$

where  $\sigma$  is the residual stress at the surface. For a Berkovich diamond indenter,  $\chi_r = 0.016 (E/H)^{1/2}$ . Since  $P$ ,  $E$ ,  $H$ , and  $c$  are all experimentally attainable from the indentation test, plotting  $P\chi_r/c^{3/2}$  against  $2(c/\pi)^{1/2}$  yields a straight line, with  $K_{IC}$  as the interception with the ordinate axis and the residual stress as the slope. This method is developed for bulk materials but has also been used to determine the fracture toughness of an organic–inorganic hybrid coating of 3–20  $\mu\text{m}$  in thickness on glass [66].

The methods described above require measurement of indentation-induced radial cracks, which is usually possible for relatively thick films. It could be difficult for thin and ultrathin ( $\leq 100$  nm) films. In the case of thin films, indentation depth usually exceeds 10% of the film thickness to generate radial cracks. As such, the elastic–plastic zone may already expand to the substrate [67,68]. Furthermore, because of the shallow indentation depths required in the indentation technique, it is often difficult to precisely measure the radial crack length even under SEM [69], presuming the indent can be located after transferring from the indenter to the SEM.

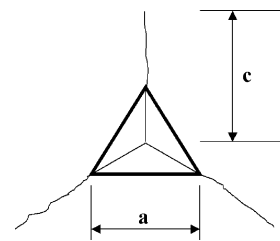


Fig. 11. Schematic diagram of median–radial crack systems for cube corner indentation.

For thin films, a more reliable approach is the energy approach [70–74]: the energy difference before and after cracking is considered responsible for fracture of the film, and the energy release rate, defined as the strain energy release per unit crack area, is calculated based on the energy difference. Once the energy release rate is obtained, toughness is obtained from  $K_c = \sqrt{EG_c}$  (for plain stress mode I fracture), or  $K_c = \sqrt{\frac{EG_c}{1-\nu^2}}$  (for plain strain mode I fracture).

As illustrated by Li et al. [69,70], fracture of hard films under a load-controlled indentation measurement may be simplified into three stages (cf. Fig. 12): (1) the first ring-like through-thickness crack forms around the indenter by high stress in the contact area; (2) delamination and buckling occur around contact area at the film/substrate interface by high lateral pressure; (3) a second ring-like through-thickness crack forms, and spalling is generated by high bending stresses at the edges of the buckled thin films.

The strain energy released in the first/second ring-like cracking and spalling can be calculated from the corresponding step in the load–displacement curve schematically shown in Fig. 13. OACD is the loading curve, and DE is the unloading curve. Area under curve ABC presents the energy difference before and after the ring-like cracking, which is released as strain energy to create the ring-like through-

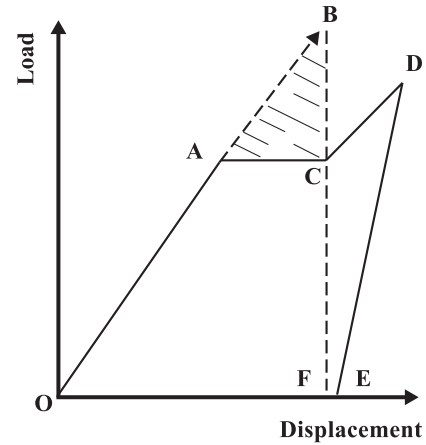


Fig. 13. Schematic diagram of a load–displacement curve showing a step during the loading cycle and associated energy release.

thickness crack. The fracture toughness of the film is then written as

$$K_{IC} = \left( \frac{E}{(1 - \nu_f^2) 2\pi C_R} \frac{\Delta U}{t} \right)^{1/2} \quad (15)$$

where  $E$  is the elastic modulus of the thin film,  $\nu_f$  the Poisson's ratio of film,  $2\pi C_R$  is the crack length in the film plane,  $t$  is the film thickness, and  $\Delta U$  is the strain energy difference before and after cracking. In this method, the cube corner indenter or the conical indenter is preferred because the through-thickness cracking of thin films can be accomplished at a low load, as demonstrated in a-C films (0.1  $\mu\text{m}$  in thickness) [75], TiN/Ti(C,N)/TiC multilayer of total thickness of 8  $\mu\text{m}$  [76], Ni/Al<sub>2</sub>O<sub>3</sub> multilayers of 0.15  $\mu\text{m}$  in thickness [77].

A somewhat similar approach was illustrated in [72,73] based on chipping (cf. Fig. 14) during indentation. The

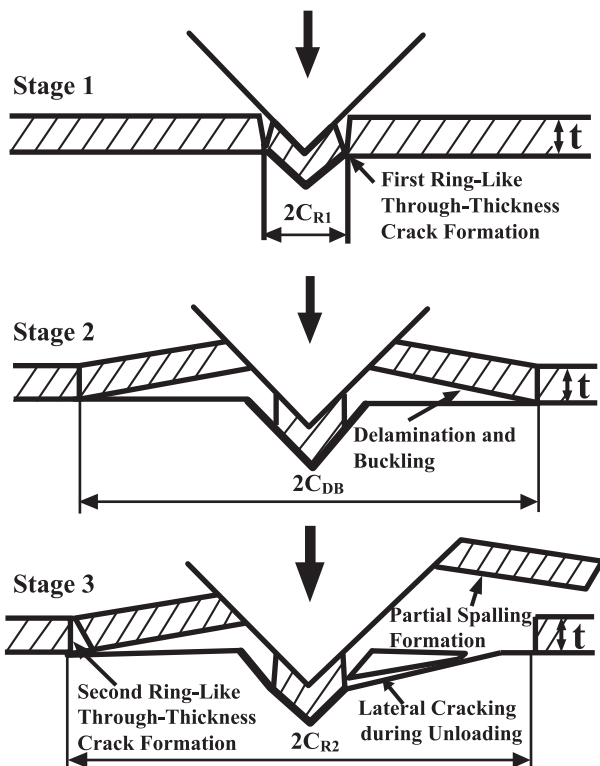


Fig. 12. Schematic of the three stages in nanoindentation fracture in a film/substrate system [69].

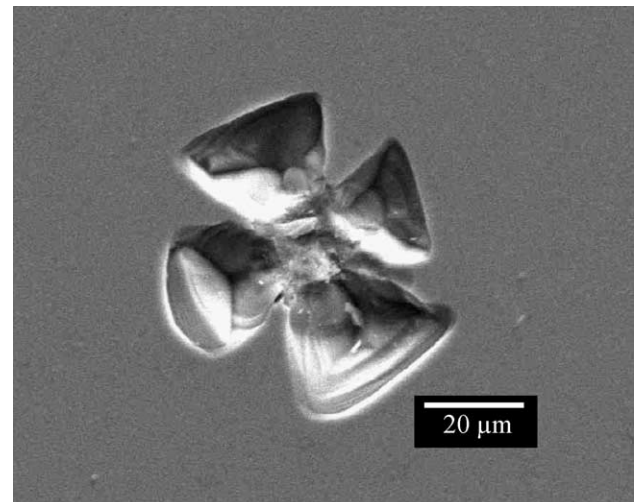


Fig. 14. The failure mode of chipping under Vickers indenter.

energy release rate during chipping under Berkovich indenter is expressed as

$$\Gamma = \frac{U_{fr}^c}{3\pi t' C_d} \quad (16)$$

where  $C_d$  is the diameter of the delamination crack that initiated the chip,  $t'$  the effective film thickness, which accounts the fact that the crack does not propagate perpendicular to the film/substrate interface.  $t'$  equals to the film thickness  $t$  divided by  $\sin(\delta)$ , where  $\delta$  is the average angle of the chipping edge.  $U_{fr}^c$  is the energy dissipated during the chipping, which can be determined from analyzing the irreversibly dissipated energy (total energy minus the elastic energy)  $W_{irr}$ .

Ignoring the thermal energy, after one indentation cycle, the irreversibly dissipated energy  $W_{irr}$  comprises the energy dissipated due to the plastic deformation ( $U_{pl}$ ) and the energy dissipated due to fracture or chipping ( $U_{fr}$ ), or

$$W_{irr} = U_{fr} + U_{pl} \quad (17)$$

$W_{irr}$  can be determined through computing the area between the loading and unloading curve. By plotting  $W_{irr}$  vs. the indentation load, a curve can be obtained (cf. Fig. 15). The onset of delamination changes the slope of the  $W_{irr}$ – $P$  curve. Before chipping takes place, the total irreversibly dissipated energy comprises that for plastic deformation ( $U_{pl}$ ) and delamination ( $U_{fr}^d$ ). Upon chipping,  $U_{fr}$  comprises two components: the energy release in delamination,  $U_{fr}^d$  and the energy released in chipping,  $U_{fr}^c$ , which is graphically attainable from the  $W_{irr}$ – $P$  curve (Fig. 15). Plugging the chipping energy back to Eq. (16) gives rise to the critical strain energy release rate, which in turn yields fracture toughness through  $K_{IC} = \sqrt{E\Gamma}$ .

Possible errors come from energy determination, crack length, and area measurement due to irregularity in crack shape. TiAlSiN thin films of hardness of 29–32.5 GPa and thickness of 2  $\mu\text{m}$  have been measured this way, and a toughness of 1.55–2.1  $\text{MPa m}^{1/2}$  is reported [78]. Malz-

bender and de With used the  $\text{SiO}_2$ -filled methyltrimethoxysilane films (thickness of 2–4  $\mu\text{m}$ ) to compare the measurements of fracture toughness by radial cracking method and the chipping method [79]. The results differ from 0 to 22%.

## 2.5. Tensile testing

For relatively thick free-standing films, fracture toughness can be directly measured using tensile method according to the ASTM standard E-399 [3], where the precrack is introduced easily by laser cutting, as in the case of diamond films with thickness of 150–200  $\mu\text{m}$  [80]. The fracture toughness of the films is thus measured as 5–6  $\text{MPa m}^{1/2}$ , comparable with those from indentation methods.

For thin films, however, measurement without creating the precrack makes more sense because of the difficulties and uncertainties involved in making precracks in micron or submicron thin films. Harry et al. [81–83] have proposed a microtensile method in which a flat rectangular substrate of dimensions  $L$  (length)  $\times$   $w$  (width)  $\times$   $h_s$  (thickness) coated with a film of thickness  $h_f$  is put under tension. In the tension process, the cracking of the film causes energy variations in the film/substrate system. For thin films ( $h_f \ll h_s$ ) coated on flat substrate ( $h_s \ll L$ ) with perfect adhesion (thus, buckling of the film will not happen), the film/substrate system can be regarded as a thin composite beam. The toughness of the film is calculated based on energy balance when the cracking occurs.

$$\Delta U = \frac{(\sigma_c^f)^2 (h_f)^2}{E^f} \left\{ \pi f \left( \frac{E^f}{E^s} \right) + \frac{\sigma_c^f}{\sqrt{3} \sigma_y^s} \right\} \quad (18)$$

where  $\Delta U$  is the net energy change,  $f(\frac{E^f}{E^s})$  is a function of the elastic modulus ratio, and the values are tabulated in Ref. [84] for different modulus ratios,  $E^f$  and  $E^s$  are the Young's modulus for film and substrate, respectively.  $\sigma_y^s$  is the yield stress of the substrate.  $\sigma_c^f$  is the effective critical cracking stress which is experimentally determined. The critical strain energy release rate for crack propagating through the film  $G_c^f$  is

$$G_c^f = \frac{\Delta U}{h_f} = \frac{(\sigma_c^f)^2 (h_f)}{E^f} \left\{ \pi f \left( \frac{E^f}{E^s} \right) + \frac{\sigma_c^f}{\sqrt{3} \sigma_y^s} \right\} \quad (19)$$

Fracture toughness of the film  $K_{IC}$  can be calculated through Eq. (3) once  $G_c^f$  is obtained. Harry et al. [81] deposited W and W–C solid solution [W(C)] films of thickness from 1.8 to 16  $\mu\text{m}$  on stainless steel substrates and subjected the film/substrate composite beams under tension and measured the fracture toughness of the W films as 1.0 to 2.5  $\text{MPa m}^{1/2}$  and that of the W(C) films as 0.2 to 1.0  $\text{MPa m}^{1/2}$ .

The major drawback of this method lies in its requirement of substrate properties. Toughness of film is in fact a property of the film itself and should not vary with substrate.

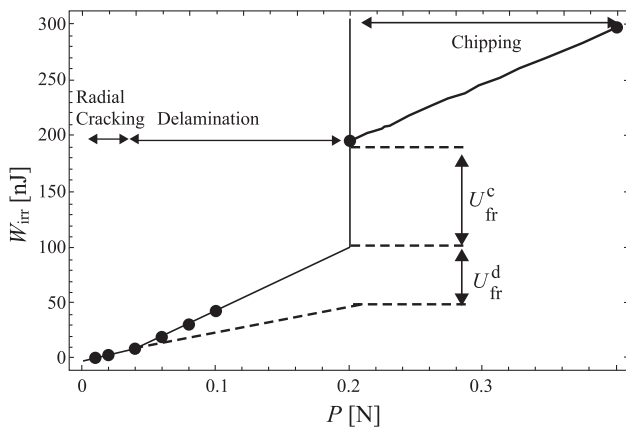


Fig. 15. Energy irreversibly dissipated during indentation as a function of the peak load applied during the indentation [72].



Zhang et al. [85] have proposed a two-step uniaxial tensile method to characterize toughness of thin hard films. In this method, the film/substrate system is subjected to uniaxial tensile stress until the film fractures, while the substrate is still elastic. After the loading is removed to allow substrate complete elastic recovery, the system is subjected to a second loading until the previous extension. The onset of film fracture is determined by the loss of linearity in the load–extension curve. Upon failure, parallel cracks are generated in the film. The crack initiation and propagation patterns are examined using SEM, and crack density (number of crack per distance) is measured. The toughness of the thin film is then derived from the energy difference between the two subsequent load–extension curves (cf. Fig. 16). Assuming that the film adheres perfectly to the substrate during loading and unloading, thus there is no interfacial cracking (i.e., no adhesion failure); the elasticity of the substrate material is good enough for it to remain elastic while cracking occurs in the film; the aspect ratio of length to thickness of the substrate is designed large enough to warrant a plain stress condition. Under the assumption of no adhesion failure, the energy variation  $\Delta U$  in the film/substrate system is attributed to the through-thickness cracking in the film, which is the area difference of  $S_{\text{OABCEO}} - S_{\text{ODEO}}$  in Fig. 16.

$$\Delta U = \int_{\text{OABCEO}} P_1(x) dx - \int_{\text{ODEO}} P_2(x) dx \quad (20)$$

That can be experimentally determined and then related to strain energy release rate. The energy release rate  $G_c$  is defined as the strain energy release per unit crack area [70,86]:

$$G_c = \frac{1}{2} \left( \frac{1}{w\rho L f(\theta)} \right) \left( \frac{dU}{dC} \right) \quad (21)$$

where  $\rho$  is the crack density or number of cracks per unit length (crack/ $\mu\text{m}$ ) obtainable from the corresponding SEM observations.  $w$  is the substrate width,  $L$  is the substrate length, thus  $w\rho L$  is the total crack length in the film plane,

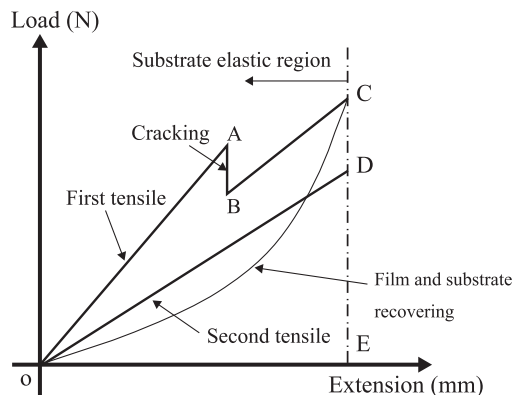


Fig. 16. Schematic diagram of load–extension curve obtained using the two-step uniaxial tensile test under extension-control [85].

$f(\theta)$  is a dimensionless factor dependent on crack orientation ( $f(\theta) \geq 1$ ). For cracks perpendicular to the film/substrate interface,  $f(\theta) = 1$ . For thin film, the through-thickness cracks propagate instantaneously, and the cracking is a single event, i.e.,  $dU/dC = \Delta U/h_f$  [70], and, when the cracks are perpendicular to the interface, Eq. (21) is rewritten as

$$G_c = \frac{1}{2} \left( \frac{1}{w\rho L} \right) \left( \frac{\Delta U}{h_f} \right) \quad (22)$$

where  $h_f$  is the film thickness,  $2w\rho Lh_f$  is the total crack area;  $\Delta U$  is the strain energy difference before and after cracking. Since the film is in plain stress condition under Mode I fracture, Eq. (3) holds. Plugging Eq. (22) into Eq. (3) gives rise to toughness  $K_C$  as

$$K_C = \left[ \left( \frac{E}{2w\rho L} \right) \left( \frac{\Delta U}{h_f} \right) \right]^{1/2} \quad (23)$$

where  $E$  is the Young's modulus of the thin film. A case study of hard nanocomposite nc-TiN/a-SiN<sub>x</sub> films of 3.0  $\mu\text{m}$  thick gives a toughness value of 2.6 MPa m<sup>1/2</sup> [85].

The advantage of this two-step tensile method lies in its independence from substrate properties, the ease, and speed in experimentation. The principle of the method, data treatment, and sample preparations are simple. In addition, the tensile test covers more area, and the property thus characterized is more close to the material intrinsic property compared with the indentation or bending methods. The drawback of the method is the elasticity requirement of the substrate: the substrate has to remain in elastic deformation, while the coated film has undergone fracture. The second important requirement is the perfect adhesion between film and substrate, without which significant variation in experiment results may occur.

### 3. Summary and ending remarks

Toughness measurement for thin films is difficult due to the small dimension in thickness. Until now, there is neither standard procedure nor standard methodology. As in qualitative or semiquantitative assessment, sometimes a quick plasticity measurement or a scratch adhesion test (for crack propagation resistance) will suffice. But these test results should not be termed "toughness."

More elaborate quantitative measurements can be categorized into two main groups: the stress approach and the energy approach. The stress approach examines the stress state near the tip of the crack. Toughness is obtained through  $K_{C\alpha}\sigma_f \sqrt{a}$ . Bending with precrack, scratch in consideration of critical tensile stress, crack length and spacing, and indentation in consideration of the critical load and corresponding crack length, etc., fall into this category. Difficulties in these methods lie in the formation of the precrack, determination of the crack length, and the critical

failure stress. These problems are not easily resolved due to the thickness dimension involved.

The energy approach concentrates on the system's energy state before and after fracture of the film. This energy difference is considered consumed to increase new crack area. Toughness is thus obtained through the critical energy release rate  $G_c$ :  $K_C = \sqrt{EG_c}$  (for plain stress mode I fracture) or  $K_C = \sqrt{\frac{EG_c}{1-\nu^2}}$  (for plain strain mode I fracture), where  $G_c$  is related to the energy difference ( $\Delta U$ ) and crack area ( $\Delta A$ ) through  $G_c \propto \Delta U / \Delta A$ . Fallen under this category are bending without precrack in the film, buckling, indentation with chipping, tensile tests, and so on.

Standardization of thin film toughness measurements seems necessary. Energy-based methodologies have clear advantages over stress-based approach.

In order not to confuse with the classical concept of fracture toughness, it is strongly suggested that the term “fracture toughness” not be used in thin film toughness description where precrack is not involved. Instead, simply, “toughness” should suffice.

## Acknowledgement

This work was supported by Nanyang Technical University's research grant RG12/02.

## References

- [1] G.E. Dieter, *Mechanical Metallurgy*, 2nd ed., McGraw-Hill, 1976.
- [2] W.D. Callister Jr., *Materials Science and Engineering an Introduction*, 6th ed., New York, Wiley, 2003.
- [3] Standard Test for Plane Strain Fracture Toughness of Metallic Materials, ASTM E-399, American Society for Testing and Materials, Philadelphia, PA, 1987.
- [4] G.P. Cherepanov, *Mechanics of Brittle Fracture*, McGraw-Hill, 1979.
- [5] D.K. Leung, M.Y. He, A.G. Evans, *J. Mater. Res.* 10 (1995) 1693.
- [6] Z. Jiang, F.X. Lu, W.Z. Tang, S.G. Wang, Y.M. Tong, T.B. Huang, J.M. Liu, *Diamond Relat. Mater.* 9 (2000) 1734.
- [7] G. Jaeger, I. Endler, M. Heilmair, K. Bartsch, A. Leonhardt, *Thin Solid Films* 377–378 (2000) 382.
- [8] G. Gille, K. Wetzig, *Thin Solid Films* 110 (1983) 37.
- [9] G. Gille, *Thin Solid Films* 111 (1984) 201.
- [10] L.C. Cox, *Surf. Coat. Technol.* 36 (1988) 807.
- [11] H. Ollendorf, D. Schneider, Th. Schwarz, G. Kirchhoff, A. Mucha, *Surf. Coat. Technol.* 84 (1996) 458.
- [12] J. Von Stebut, F. Lapostolle, M. Bucsa, H. Vallen, *Surf. Coat. Technol.* 116–119 (1999) 160.
- [13] D. Almond, M. Moghisi, H. Reiter, *Thin Solid Films* 108 (1983) 439.
- [14] P.M. Ramsey, H.W. Chandler, T.F. Page, *Thin Solid Films* 201 (1991) 81.
- [15] U. Wiklund, P. Hedenqvist, S. Hogmark, *Surf. Coat. Technol.* 97 (1997) 773.
- [16] C.E. Kalnas, J.F. Mansfield, G.S. Was, J.W. Jones, *J. Vac. Sci. Technol.*, A 12 (3) (1994) 883.
- [17] U. Wiklund, M. Bromark, M. Larsson, P. Hedenqvist, S. Hogmark, *Surf. Coat. Technol.* 91 (1997) 57.
- [18] B. Cotterell, Z. Chen, *Int. J. Fract.* 104 (2000) 169.
- [19] Z. Chen, B. Cotterell, W. Wang, *Eng. Fract. Mech.* 69 (2002) 597.
- [20] S.J. Britvec, *The Stability of Elastic Systems*, Pergamon Press, New York, 1973.
- [21] J.W. Hutchinson, *Mechanics of Thin Films and Multilayers*, Technical University of Denmark, 1996.
- [22] J.J.L. Beuth, *Int. J. Solids Struct.* 29 (1992) 1657.
- [23] V. Bellido-Gonzalez, N. Stefanopoulos, F. Deguilhen, *Surf. Coat. Technol.* 74–75 (1995) 884.
- [24] X. Li, B. Bhushan, *J. Mater. Res.* 14 (6) (1999) 2328.
- [25] S. Sundararajan, B. Bhushan, *J. Mater. Res.* 16 (2) (2001) 437.
- [26] Peter Panjan, Miha Cekada, Boris Navinsek, *Surf. Coat. Technol.* 174–175 (2003) 55.
- [27] A.A. Voevodin, C. Rebholz, J.M. Schneider, P. Stevenson, A. Matthews, *Surf. Coat. Technol.* 73 (1995) 185.
- [28] E. Harry, A. Rouzaud, P. Juliet, Y. Pauleau, M. Ignat, *Surf. Coat. Technol.* 116–119 (1999) 172.
- [29] A.A. Voevodin, J.S. Zabinski, *Thin Solid Films* 370 (2000) 223.
- [30] A.A. Voevodin, J.S. Zabinski, *J. Mater. Sci.* 33 (1998) 319.
- [31] P.W. Shum, K.Y. Li, Z.F. Zhou, Y.G. Shen, *Surf. Coat. Technol.* 185 (2004) 245.
- [32] J. Ligot, S. Benayoun, J.J. Hantzpergue, *Wear* 243 (2000) 85.
- [33] S. Zhang, D. Sun, Y.Q. Fu, H. Du, *Thin Solid Films* 447–448 (2004) 462.
- [34] J.W. Hoehn, S.K. Venkataraman, H. Huang, W.W. Gerberich, *Mater. Sci. Eng., A* 192–193 (1995) 301.
- [35] K. Holmberg, A. Laukkanen, H. Ronkainen, K. Wallin, S. Varjus, *Wear* 254 (2003) 278.
- [36] Yu. V. Milman, B.A. Galanov, S.I. Chugunova, *Acta Metall. Mater.* V41 (9) (1993) 2523.
- [37] A.A. Voevodin, M.S. Donley, *Surf. Coat. Technol.* 82 (1996) 199.
- [38] A.A. Voevodin, S.V. Prasad, J.S. Zabinski, *J. Appl. Phys.* 82 (2) (1997) 855.
- [39] S. Zhang, X.L. Bui, Y.Q. Fu, *Surf. Coat. Technol.* 167 (2003) 137.
- [40] T.Y. Tsui, J.V. Vlassak, M.D. Nix, *J. Mater. Res.* 14 (1999) 2204.
- [41] T.Y. Tsui, Y. Joo, *Thin Solid Films* 401 (2001) 203.
- [42] A.A. Wells, *Br. Weld. J.* 10 (1963) 563.
- [43] J. Malzbender, G. de With, *Surf. Coat. Technol.* 137 (2001) 72.
- [44] J. Malzbender, G. de With, *Surf. Coat. Technol.* 127 (2000) 265.
- [45] R. McGurk, T.F. Page, *J. Mater. Res.* 14 (1999) 2283.
- [46] H. Holleck, H. Schulz, *Surf. Coat. Technol.* 36 (1988) 707.
- [47] F. Kustas, B. Mishra, J. Zhou, *Surf. Coat. Technol.* 120–121 (1999) 489.
- [48] B.R. Lawn, A.G. Evans, D.B. Marshall, *J. Am. Ceram. Soc.* 63 (1980) 574.
- [49] G.R. Anstis, P. Chantikul, B.R. Lawn, D.B. Marshall, *J. Am. Ceram. Soc.* 64 (1981) 533.
- [50] G.M. Pharr, D.S. Harding, W.C. Oliver, in: M. Nastasi, Don M. Parkin, H. Gleiter (Eds.), *Mechanical Properties and Deformation Behavior of Materials Having Ultra-Fine Microstructure*, Klumer Academic Press, 1993, p. 449.
- [51] A. A. Volinsky, J. B. Vella, W. W. Gerberich, *Thin Solid Films* 429 (2003) 201.
- [52] W.C. Oliver, G.M. Pharr, *J. Mater. Res.* 7 (1992) 1564.
- [53] G.M. Pharr, *Mater. Sci. Eng., A* 253 (1998) 151.
- [54] A.E. Giannakopoulos, P.-L. Larsson, R. Vestergaard, *Int. J. Solids Struct.* V31 (19) (1994) 2679.
- [55] W.C. Oliver, G.M. Pharr, *J. Mater. Res.* V19 (1) (2004) 3.
- [56] T. Lube, T. Fett, *Eng. Fract. Mech.* 71 (2004) 2263.
- [57] D.S. Harding, W.C. Oliver, G.M. Pharr, *Mater. Res. Soc. Symp. Proc.* 356 (1995) 663.
- [58] T.W. Scharf, H. Deng, J.A. Barnard, *J. Vac. Sci. Technol.*, A 15 (3) (1997) 963.
- [59] P. Kodali, K.C. Walter, M. Nastasi, *Tribol. Int.* V30 (8) (1997) 591.
- [60] Y. Xie, H.M. Hawthorne, *Wear* 233–235 (1999) 293.
- [61] X. Li, B. Bhushan, *Thin Solid Films* 340 (1999) 210.
- [62] P. Jedrzejowski, J.E. Klemberg-Sapieha, L. Martinu, *Thin Solid Films* 426 (2003) 150.

- [63] P. Jedrzejowski, J.E. Klemberg-Sapieha, L. Martinu, *Thin Solid Films* 466 (2004) 189.
- [64] T. Fett, *Eng. Fract. Mech.* V52 (4) (1995) 773.
- [65] D.B. Marshall, B.R. Lawn, *J. Am. Ceram. Soc.* 60 (1977) 86.
- [66] J. Malzbender, G. de With, J.M.J. den Toonder, *Thin Solid Films* 366 (2000) 139.
- [67] T. W. Scharf, H. Deng, J. A. Barnard, *J. Vac. Sci. Technol., A* 15 (3) (1997) 963.
- [68] Z. Xia, W.A. Curtin, B.W. Sheldon, *Acta Mater.* 52 (2004) 3507.
- [69] X. Li, D. Diao, B. Bhushan, *Acta Mater.* 45 (11) (1997) 4453.
- [70] X. Li, B. Bhushan, *Thin Solid Films* 315 (1998) 214.
- [71] B. Bhushan, *Diamond Relat. Mater* 8 (1999) 1985.
- [72] J.D. Toonder, J. Malzbender, G.D. With, R. Balkenende, *J. Mater. Res.* 17 (1) (2002) 224.
- [73] J. Malzbender, G. de With, *Surf. Coat. Technol.* 135 (2000) 60.
- [74] J. Malzbender, J.M.J. den Toonder, A.R. Balkenende, G. de With, *Mater. Sci. Eng.* R36 (2002) 47.
- [75] X. Li, B. Bhushan, *Thin Solid Films* 355–356 (1999) 330.
- [76] J. Ding, Y. Meng, S. Wen, *Thin Solid Films* 371 (2000) 178.
- [77] S. Neralla, D. Kumar, S. Yarmolenko, J. Sankar, *Composites, Part B* 35 (2004) 157.
- [78] O. Nakonechna, T. Cselle, M. Morstein, A. Karimi, *Thin Solid Films* 447–448 (2004) 406.
- [79] J. Malzbender, G. de With, *J. Non-Cryst. Solids* 265 (2001) 51.
- [80] M.D. Drory, R.H. Dauskardt, A. Kant, R.O. Ritchie, *J. Appl. Phys.* 78 (5) (1995) 3083.
- [81] E. Harry, A. Rouzaud, M. Ignat, P. Juliet, *Thin Solid Films* 332 (1998) 195.
- [82] E. Harry, M. Ignat, Y. Pauleau, A. Rouzaud, P. Juliet, *Surf. Coat. Technol.* 125 (2000) 185.
- [83] E. Harry, M. Ignat, A. Rouzaud, P. Juliet, *Surf. Coat. Technol.* 111 (1999) 177.
- [84] M.S. Hu, A.G. Evans, *Acta Metall.* 37 (3) (1989) 917.
- [85] S. Zhang, D. Sun, Y.Q. Fu, H. Du, *Thin Solid Films* (2004) (in press).
- [86] B.R. Lawn, *Fracture of Brittle Solids*, 2nd ed., Cambridge University Press, Cambridge, U.K., 1993.